RESEARCH PAPER

SOLID-STATE DIFFUSION BONDING OF X70 STEEL TO DUPLEX STAINLESS STEEL

Lamia Baghdadi[1], Zakaria Boumerzoug[1], François Brisset[2], Denis Solas[2], Thierry Baudin[2]*

[1]*LMSM, Mechanical Engineering Department, University of Biskra, B.P. 145, 07000, Biskra, Algeria*
[2]*Université Paris-Saclay, CNRS, Institut de chimie moléculaire et des matériaux d'Orsay, 91405 Orsay, France*

Corresponding author: Zakaria Boumerzoug, email:z.boumerzoug@uni-biskra.dz, tel.: +2131151596994, LMSM, Mechanical Engineering Department, University of Biskra, B.P. 145, 07000, Biskra

ABSTRACT

This paper deals with the solid-state diffusion bonding of X70 steel to duplex stainless steel. Microstructure and mechanical properties of the welded dissimilar steels were investigated. Optical microscopy, Electron Backscatter Diffraction, energy dispersive spectrometry, Vickers hardness measurements, and X-Ray Diffraction were the main techniques of characterization. Microstructural variation was observed in the X70 steel side compared to duplex stainless steel. The diffusion coefficient of iron, chromium, and nickel across the interface X70 steel/duplex stainless steel was also measured. The diffusion coefficient of iron and chromium is higher than that of nickel. The Vickers microhardness profile across the bond joint showed an abrupt decrease in hardness from duplex stainless steel to X70 steel. In addition, a dynamic recrystallisation reaction was observed close to the interface on the X70 steel side.

Keywords:solid-state diffusion; X70 steel; duplex stainless steel; interface; microstructure

INTRODUCTION

The subject of dissimilar metal welding covers a wide range of materials and production techniques. Better knowledge of dissimilar joining processes allows industries to create more durable products that use less energy and are easier to recycle [1]. Welding dissimilar steels is a challenge in the manufacture of the power generation industries and many types of equipment used in the petrochemical and oil fields [2, 3]. However, welding of dissimilar materials is more complex than that of similar materials due to differences in the physical, chemical, mechanical and metallurgical properties of the base materials [4].

Among the steels of wide industrial use, there is the duplex stainless steel which for certain industrial obligations it is welded to ordinary steel. Duplex stainless steel (DSS), with an almost equal proportion of ferrite and austenite phases, perfectly combines most of the beneficial properties of austenitic stainless steel (ASS) and ferritic stainless steel (FSS), including high strength, good toughness and excellent corrosion resistance [5-7].

The joining of duplex stainless steels to low carbon or low alloy steels is often used in the petroleum, petrochemical, nuclear and marine industries, due to their perfect combination of high tensile strength, good toughness, and adequate weldability and stress corrosion resistance [8-10]. With the development of deepwater oil and gas exploitation, more and more duplex stainless steels have been used in the flowline. However, low alloy steels are used in the cold end flowline section for economic considerations. Therefore, dissimilar solder joints are an industrial necessity [11].

The main practical techniques used to join duplex stainless steels to carbon steels were either explosive welding [12] or tungsten welding under inert gas [13, 14]. However, solid-state bonding is considered an alternative technique for joining dissimilar steels for special purposes where conventional welding is not suitable [15]. Solid-state processes are classes of welding techniques that produce mating surface assembly at temperatures below the melting point of the base metals being joined without the addition of solder filler metal. In this process, pressure may or may not be used. This class includes forge welding, roll welding, explosion welding, diffusion welding, friction welding, hot pressure welding, and ultrasonic welding [16].

Diffusion bonding is a solid-state joining process, used to join similar and dissimilar materials without high microscopic deformation and with minimal dimensional tolerances [17, 18]. The principle of solid-state diffusion is based on the interdiffusion of atoms across the contact surface between two metals. This is usually done at a high temperature, around 50-75% of the material absolute melting temperature [19, 20]. Temperature, pressure and bonding time are the three main parameters in the diffusion bonding process [21]. The main advantage of this process is that the joined metals retain their original properties without the development of a heat affected zone as in the conventional welding process [22].

Based on literature data, a limited number of published works are available on diffusion welding of similar or dissimilar steels. Derby and Wallach [23] carried out research work on the comprehension of the mechanism of diffusion bonding in steel. They concluded that the dominant mechanism for diffusion bonding of iron was found to be surface diffusion initially, although other mechanisms result in the eventual closure of voids in the contact surface. This shows that the preparation of the surface before bonding is important. Gawde et al. [15] investigated the diffusion bonding of similar stainless steels

using intermediate layers of Ni, Cu, and Ag. Results indicated the absence of brittle intermetallics at the interfaces. Masahashi et al. [24] studied the diffusion bonding of a couple of Fe-Al alloy and high-carbon steel. They observed a columnar microstructure at the joint interface. Sharma et al. [21] studied the application of an impulse pressure-assisted diffusion bonding of low carbon steel with the incorporation of silver as an interlayer. They found that the bonding temperature was the most significant parameter for developing a sound diffusion bond. Zhang et al. [26] bonded stainless steel to carbon steel using a diffusion process with a plastic deformation by compression. They found that with an increase in deformation temperatures, the bonding efficiency also increases significantly. Cox et al. [26] conducted bonding experiments on similar AISI 304 austenitic stainless steel in a very well controlled chemical environment with low applied loads. They found that a chemically clean austenitic stainless steel with low microscopic roughness can be completely diffusion bonded with low loads in 1 hour at 1000 ^{0}C. Kurt and Calik [27] studied the interface structure of diffusion bonded (between 750 and 900 ^{0}C) duplex stainless steel and medium carbon steel couple. They observed mutual diffusion of chromium and carbon which caused the formation of a carbide layer at the interface.

Among these research works, the scientific investigation of Wang et al. [11] is the only available published work on the joining of duplex stainless steel to X70 steel, but by inert gas (MIG) welding and tungsten inert gas (TIG) welding processes. They investigated the effect of the welding process on the microstructure and properties of dissimilar solder joints. They found more austenite present in the weld metal by MIG welding than in TIG welding, and the austenite content increases in the weld metal compared to the DSS base metal, which is beneficial for the mechanical properties and the corrosion resistance.

Based on this literature review, it becomes interesting to investigate the solid-state diffusion bonding of X70 steel to duplex stainless steel. The microstructures and the mechanical properties of the dissimilar steels were studied. The diffusion mechanisms through the interface were also discussed.

MATERIAL AND METHODS

Base metals used in this work are low alloy steel (X70) and duplex stainless steel which are used in pipeline construction for gas and oil transport. The nominal chemical composition of these dissimilar steels is given in **Table 1**.

Table 1 Nominal chemical composition (Wt. %) of X70 steel and duplex stainless steel.

Material	C	Si	Mn	P	Cr	Ni	Mo	Fe	Other elements
X70	0.07	0.20	1.02	0.02	0.05	0.06	0.15	98.00	0.43
DSS	0.02	1.50	1.54	0.02	20.00	6.65	2.01	67.00	1.26

Before the solid-state diffusion bonding process, the surface samples were polished using SiC papers with grain sizes of 600, 800, 1200, and 2400. Then, the polished samples were cleaned with ethanol. The schematic diagram of the diffusion bonding configuration is shown in **Fig.1**. The two dissimilar sheets of steel were fixed by a loading device equipped with a tightening screw to exert a homogeneous pressure (**Fig.1**). It is noted that the pressure was kept constant. Diffusion bonding was carried out at 1150 °C in a vacuum chamber for 5 hours.
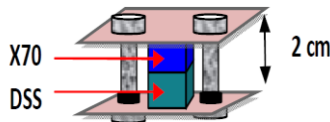

Fig 1. Schematic configuration of the diffusion bonding of the dissimilar steels.

After bonding, the bonded specimens were cut perpendicular to the joining surface (interface) and as a final step, they were metallographically polished with 3 μm diamond paste. For the microstructural examination, the X70 steel was etched with 2 % nital for 20 s and duplex stainless steel was etched with a chemical solution containing 5 g CuCl$_2$, 100 ml HCl, and 100 ml Alcohol.

For Electron Back Scattered Diffraction (EBSD) analysis, specimens were prepared using the standard sample preparation method (mechanical polishing with a 2400 grade emery paper, followed by OPS polishing).A Zeiss Supra 50 FEG-SEM operating at 20 kV coupled with the automatic OIM^{TM} (Orientation Imaging Microscopy) software from TSL-EDAX Company was used for the sample cross-section EBSD analyses. Moreover, SEM is equipped with energy dispersive spectroscopy (EDS) that was used to characterize the diffusion of chemical elements across the interface.

The Vickers hardness across the weld joint was measured by Digital Micro-Vickers Hardness Tester type HVS-1000 Z using a 0.3 kg load. In addition, X-Ray Diffraction (XRD) was used

to determine the main phases in base metals and welded dissimilar steel. The INEL CPS 120 curved detector was used. The experimental parameters were a Co tube (0.17902 nm) operating at 30 kV and 22.5 mA. The X-ray source beam spot size was 1 mm. The samples orientation angles were χ from 0° to 45° step 5°, φ from 0 to 355° step 5°, and angle of incidence ω=30°. The diffractograms correspond to the sum of the diffractograms measured for the different orientations of the sample.

RESULTS AND DISCUSSION

Microstructural observation

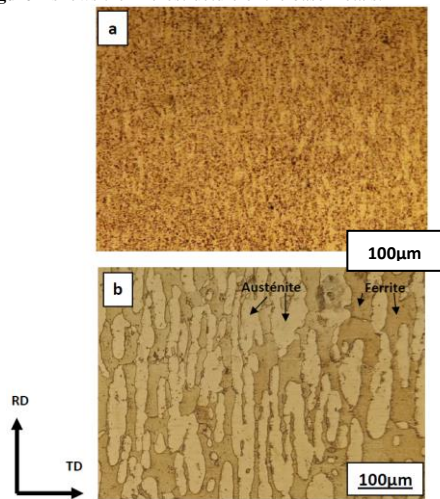**Figure 2** shows the microstructure of the base metals.

Fig. 2 Microstructure of the dissimilar steels (a): X70 steel, and (b): duplex stainless steel.

The microstructure of X70 steel (**Fig. 2a**) consists of ferrite which is the predominant phase and small colonies of pearlite (α-Fe + Fe₃C). The grain size of ferrite is approximatively equal to 50 µm. The microstructure of duplex stainless steel (**Fig. 2b**) is composed of elongated ferrite and elongated austenite in equal quantities. The elongated grains in duplex stainless steel were the result of the hot rolling process during the industrial manufacturing of the pipe.

Welded joint

The optical micrograph of dissimilar joint, X70 steel with duplex stainless steel welded by a solid-state diffusion bonding process at 1150C for 5h is shown in **Fig. 3**. The interface is straight and no defects were observed such as pores or cracks. Moreover, a thin layer is observed at the interface. However, microstructural changes were observed in both base metals. On the duplex stainless steel side, the grains do not retain their elongated shape and become equiaxed with a grain size of the order of 20 µm.The majority of the colonies of pearlite on the X70 steel side have submitted dispersion in ferritic grains. Moreover, grain growth is observed close to the interface, where the grain size is more than 100 µm. Cette croissance de grains semble liée à la disparition de la perlite sur une distance de l'ordre de 200µm par rapport à l'interface. On peut donc supposer une diffusion du carbone sur cette distance. En effet, le carbone diffuse plus vite que les autres éléments et on voit sur la figure 4 que ceux-ci diffusent sur une distance de l'ordre de 60-70µm.

All these phenomena are due to the bonding temperature which is considered a very high temperature which accelerates the diffusion process and leads both to the rearrangement of the grains and recrystallization reaction. It has been noticed Shiwei et al.[28] the effect of bonding temperature on the microstructural evolution of the base metals. They observed a coarsening of grains and some precipitates after the diffusion-bonding of CoCrNi-based medium-entropy alloy to DD5 single-crystal superalloy.

Fig. 3 Microstructures of the dissimilar weld of duplex stainless steel with X70 steel, joined by solid-state diffusion bonding process at 1150 °C for 5 h.

Figure 4 presents the EDS analysis across welded duplex stainless steel / X70 steel, where the concentration variation curves of the chemical elements likely to diffuse through the interface joint have been plotted: silicon, molybdenum, cobalt, iron, chromium, and nickel.

According to the concentration variation curves, the diffusion of silicon, molybdenum and silicon is almost negligible. The two main elements which continuously diffuse through the interface are iron and chromium. On the contrary, the diffusion of nickel is more or less slow. During this welding process, the interdiffusion of atoms across the interface represents the main mechanism to weld the two dissimilar sheets of steel.
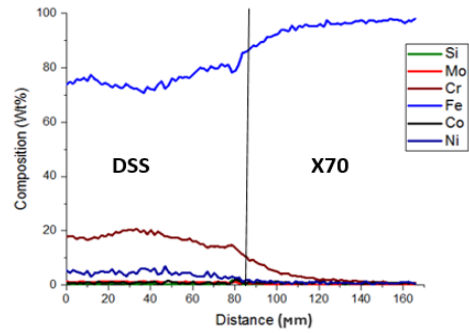

Fig. 4 EDS analysis across the interface of the dissimilar joint duplex stainless steel with X70 steel, joined by solid-state diffusion bonding process at 1150 °C for 5 h.
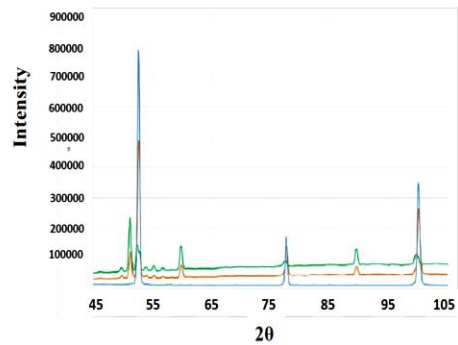

Fig. 5 X-ray diffractograms in each zone of the welded joint. (Omega = 30° Chi 0 à 70 / 5°, Phi 0 à 355 / 5°). The blue curve in X70 steel, the Green curve in DSS, and the Orange curvein a welded joint.
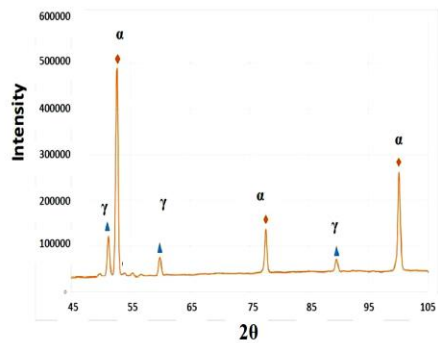

Fig. 6 X-ray diffractogram in the central zone of the welded joint.

Based on the interdiffusion process between the two dissimilar sheets of steel, X-ray diffraction analyzes were performed on the welded joint to determine if there is the formation of new phases. **Figure 5** shows the X-ray diffractograms in each zone of the welded joint. The X-ray diffractogram of the X70 steel (Blue curve) reveals the peaks of ferritic phase α (Blue curve).

The X-ray diffractogram of the duplex stainless steel (Green curve) reveals the peaks of ferritic phase α with austenitic phase γ with new peaks in low diffraction angles. However, the X-ray diffractogram of the central zone of the welded joint (Orange curve) shows the presence of peaks observed in the two dissimilar metals. **Figure 6** presents the X-ray diffractogram of the central zone of the welded joint with the main revealed phases (α: Ferrite and γ: Austenite). Therefore, the solid-state diffusion welding process of these two dissimilar sheets of steel did not cause the formation of new phases at the interface, which will allow to obtain of a joint of good mechanical properties.

Diffusion coefficients

The second law of Fick for unidirectional flow under steady-state conditions is written as:

$$\frac{\partial c}{\partial t} = \frac{\partial}{\partial x}\left(D\,\frac{\partial c}{\partial x}\right) \tag{1.}$$

If Cx is the concentration of an element at distance 'x' from the interface, the second law of Fick is rewritten as given below:

$$\frac{\partial c_x}{\partial t} = D\left(\frac{\partial^2 c_x}{\partial x^2}\right) \tag{2.}$$

The solution to this equation is:

$$C(x,t) = A - B\,erf\left(\frac{x}{2\sqrt{Dt}}\right) \tag{3.}$$

Where A and B are:

$$A = \left(\frac{C_1 + C_2}{2}\right)\ ,\ B = \left(\frac{C_1 - C_2}{2}\right) \tag{4.}$$

Where C_1 and C_2 are the initial concentrations of the elements under study in both materials. 'x' is the distance from the interface, 't' is the bonding time and 'D' is the diffusion coefficient [29].

The diffusion coefficient (*D*) is defined as the amount of a particular substance that diffuses across a unit area in 1 s under the influence of a gradient of one unit [30]. It is expressed in the units $cm^2\ s^{-1}$.

From equations (3) and (4), the expression of C(x, t) becomes:

$$C_X = \left[\frac{(C_1 + C_2)}{2}\right] - \left[\frac{(C_1 - C_2)}{2}\right]\,erf\left[\frac{x}{(2\sqrt{Dt})}\right] \tag{5.}$$

By using SEM and EDS analysis, the different elemental concentrations and distance x (30 µm) from the interface on either side of the base metals were measured (**Table 2**).In this case, there was an interdiffusion process, because the atoms of iron diffuse from the X70 steel to the DSS, however, the atoms of chromium and nickel diffuse from the DSS to X70 steel. Belkessa et al. [31] revealed a high concentration gradient of alloying elements (Cr, Ni and Mo) in welded duplex stainless steel and low alloy steel.

Table 2 The different elemental concentrations and distance x = 30 µm from the interface bonded DSS to X70 steel, joined by a solid-state diffusion bonding process at 1150 °C for 5 h.

Element	C_1 (Wt. %)	C_2 (Wt.%)	C_x (Wt.%)
Fe	98.00	67.00	74.00
Cr	20.00	00.05	14.00
Ni	06.50	00.06	03.00

Based on the measured values given in Table 2 and calculated from equation (5), the diffusion coefficient values of 'Cr', 'Ni', and 'Fe' were calculated for the same diffusion distance x = 30 µm (Table 3). In general, the width of the diffusion zone is proportional to the square root of diffusion time [32]. The first remark to be mentioned is that the diffusion coefficient is not the same for the three elements. The diffusion coefficient of iron and chromium is higher than the nickel one. This difference mainly depends on the difference in the atomic radius between Chromium (r = 0.185 nm), Iron (r = 0.172 nm), and Nickel (r = 0.162 nm), and the diffusivity of each element. Vigraman et al. [33] performed calculations of the diffusion coefficient of chromium and nickel across an interface of a joint made by diffusion welding process between duplex stainless steel and medium-carbon steel between 850 and 950 °C, which is an approximately similar case. The obtained values of the diffusion coefficients of these elements are not different from the present values.

Table 3 Diffusion coefficient values of Cr, Ni, and Fe in bonded DSS to X70 steel.

Element	**D** (m^2/s)
Fe	6.76×10^{-14}
Cr	3.47×10^{-14}
Ni	0.85×10^{-14}

Local microstructure analysis

Figure 7 presents the EBSD map of the dissimilar joint. The EBSD map shows the grain growth reaction close to the interface in the X70 steel side; however, the grain size on the DSS side is the same.
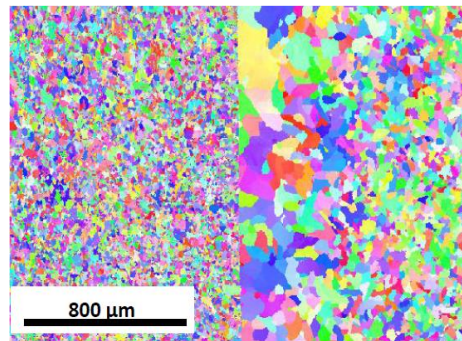

Fig. 7 EBSD "direction"-IPF map of the dissimilar joint, duplex stainless steel with X70 steel, joined by solid-state diffusion bonding process at 1150 °C for 5 h.

For more details about grain growth on the X70 steel side, **Figure 8** illustrates a phase-coloured map (**Fig. 8a**) and the grain size distribution (**Fig. 8b**), which indicates that the average grain size varies from 50 µm in the core of X70 steel to about 180 µm close to the interface. The highest grain sizes are illustrated with a red and green colour (**Fig. 8a**). The highest grain size (red colour) is located near the interface. Consequently, the interface is a preferential site for the grain growth reaction of ferritic grains. Let us note that the interface is surface contact between ductile steel (X70) and hard steel (DSS). During the bonding process, the X70 steel submits a local deformation at a high temperature from the DSS side, which leads to dynamic recrystallization on the X70 steel side.

As observed previously, the grain growth zone corresponds to that where the pearlite has disappeared in the X70 steel at the interface. Therefore, it can be assumed that there has been a diffusion of the carbon in the duplex steel. Under these conditions, this zone of the X70 steel contains less carbon. Thus, during treatment at 1150 ° C, it can be assumed that a transformation $\alpha \rightarrow \gamma$ is appeared. Thus and given the different dilation of ferritic and austenitic/ferritic materials, the plastic deformation generated in the X70 is certainly at the origin of the recrystallization and the growth of the grains.
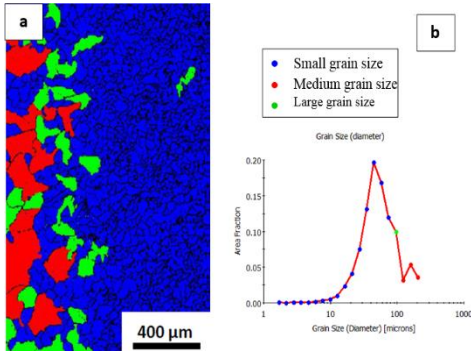

Fig. 8 (a): EBSD map and (b): grain size distribution in X70 steel side, joined to duplex stainless steel by solid-state diffusion bonding process at 1150 ^{0} C for 5 h.

Figure 9 presents the phase-coloured map of the dissimilar joint. On the DSS side, the phase-coloured map shows a homogeneous distribution of austenite (red colour) and ferrite (green colour), with a slight quantitative difference between these two phases. In addition, the X70/DSS interface appears straight and free of apparent defects.
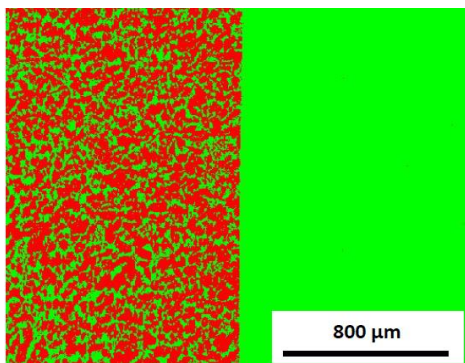

Fig. 9 Phase-colored map of the dissimilar joint, duplex stainless steel with X70 steel, joined by solid-state diffusion bonding process at 1150 ^{0}C for 5 h (Ferrite in green colour, Austenite in red colour).

.
Figure 10 shows a magnification of two selected areas in the dissimilar joint where more details can be observed. **Figures 10a** and **b** show the formation of sub-grains slightly disoriented between them (same colour on the map) characteristic of cold deformation or possibly having undergone a slight dynamic restoration to allow a rearrangement of the dislocations. Moreover, some areas at the interface are formed with a

thin (ferritic or austenitic) layer (shown by the blue arrow) (**Fig.10b**). Figure 10c presents a zoom of such a thin layer with a higher resolution that shows the fine substructure described above.

Figure 10a shows also the growth of a small grain at the interface (red arrow) from the DSS to the X70 steel. In this case, it is a ferritic grain but austenitic grains have been observed too. In addition to the atomic interdiffusion across the interface, these phenomena contribute to the strengthening of the bonding process between the two dissimilar sheets of steel. Yu et al. [34] revealed by EBSD technique, a growth of small new grains at the interface during a diffusion bonding of Cr ferrite heat-resistant steel to austenitic heat-resistant steel. They attributed this phenomenon to the deformation of storage energy and dislocation slips in the interface.
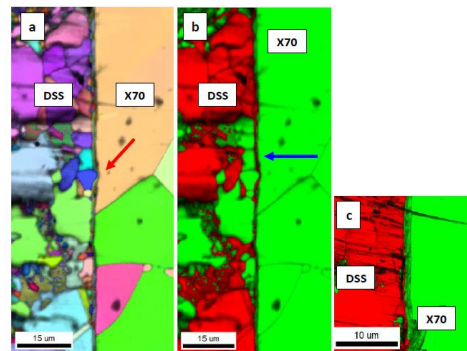

Fig. 10 EBSD maps of the dissimilar joints, duplex stainless steel with X70 steel, joined by solid-state diffusion bonding process at 1150 ^{0} C for 5 h. (a) –DN-IPF, (b) and (c) phase maps (green = ferrite and red = austenite)

Hardness Test
Hardness measurements are the usual technique for evaluating the properties of the welded joint [35]. In this context, the hardness curve through the welded joint was drawn from the DSS steel to the X70 steel (**Fig.11**). As expected, the hardness values in DSS (350 Hv) are higher than in X70 steel (125 Hv).
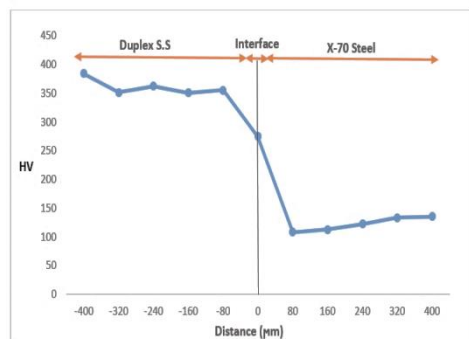

Fig. 11 Microhardness distribution across the bond interface of the dissimilar weld joint, duplex stainless steel with X70 steel, joined by solid-state diffusion bonding process at 1150 ^{0} C for 5 h.

However, the hardness in the central area has intermediate hardness values (150-300 Hv). These intermediate values can be attributed to the process of atomic interdiffusion and recrystallization reaction in the interfaceduring thesolid-state diffusion bonding process. Vigraman et al. [33], attributed the hardness variation at the centre of the welded joints, to the migration of atoms from either side of the diffusion couple duplex stainless steel/medium-carbon steel. Finally, let us remark that the hardness is quite the same in the area of large grains in the X70 steel. This could be due to the diffusion of alloy elements in this zone.

CONCLUSIONS

In summary, this study is a contribution to the investigation of the welding of dissimilar steels (X70 and Duplex stainless steels) by the solid-state diffusion bonding process. Optical microscopy, EDS analysis, X-ray analysis, EBSD technique, and hardness measurements were the main techniques of characterization.
The main conclusions are as follows:

- The solid-state diffusion welding technique can be successfully applied to joining X70 and duplex stainless steel.
- Interface in the welded joint has been formed between the dissimilar materials.
- The interdiffusion process is the main mechanism during the solid-state diffusion bonding at 1150 ^{0}C. The diffusion welding process of these two dissimilar sheets of steel did not cause the formation of new phases at the interface.
- Iron and chromium atoms are the main atoms that diffuse across the interface, with a lesser degree nickel atoms. Both iron and chromium have high diffusion coefficient values
- A grain growth reaction was observed near the interface of the X70 steel side.
- The hardness measurement confirmed both the interdiffusion process and grain growth during the bonding process.

REFERENCES

1. D. K. Singh, V. Sharma, R. Basu, M. Eskand: Procedia Manufacturing, 35, 2019, 986–991. https://doi.org/10.1016/j.promfg.2019.06.046.
2. A. Josepha, S. K. Raib, T. Jayakumara, N. Muruganc: International Journal of Pressure Vessels and Piping, 82, 2005, 700–705. https://doi.org/10.1016/j.ijpvp.2005.03.006.
3. N. Arivazhagan, S. Singh, S. Prakash, G. M. Reddy: The International Journal of Advanced Manufacturing Technology, 39, 2008, 679–689. https://doi.org/10.1007/s00170-007-1266-7.
4. D. Xinjie, Z. Zhong, C. Denga, D. Wang, G. Xiaojiang: Materials and Design, 95, 2016, 231–236. https://doi.org/10.1016/j.matdes.2016.01.087.
5. D. Lacerda, J.C. Candido, L. Godefroid: International Journal of Fatigue, 74, 2015, 81–87. https://doi.org/10.1016/j.ijfatigue.2014.12.015.
6. Z. Zhang, H. Jing, X. Lianyong , Y. Han, L. Zhao, J. Zhang less: Applied Surface Science, 394, 2017, 297–314. https://doi.org/10.1016/j.apsusc.2016.10.047.
7. F. Mirakhorli, F. MalekGhaini, M. Torkamany: Journal of Materials Engineering and Performance, 21, 2012, 2173–2176. https://doi.org/10.1007/s11665-012-0141-3.

8.R. Merello, F.J. Botana, J. Botella, M.V.Matres, M. Marcos:Corrosion Science45, 2003, 909–921. https://doi.org/10.1016/S0010-938X(02)00154-3.
9. N.R. Baddoo: Journal of Constructional Steel Research, 64, 2008, 1199–1206. https://doi.org/10.1016/j.jcsr.2008.07.011.
10. B. Elsener, D. Addari, S. Coray, A. Rossi: Materials and Corrosion, 62, 2011, 111–119. http://dx.doi.org/10.1002/maco.201005826.
11. J. Wang, M. Lu, L. Zhang, W. Chang, X. L. Xu, L. Hu: International Journal of Minerals, Metallurgy and Materials, 19, 2012, 518. https://doi.org/10.1007/s12613-012-0589-z.
12. R. Kaçar, M. Acarer: Materials Science and Engineering A, 363, 2003, 290–296. http://dx.doi.org/10.1016/S0921-5093(03)00643-9.
13. Y. Zou, U. Rintaro, F. Hidetoshi: Materials Science and Engineering A, 620, 2015, 140-148 https://doi.org/10.1016/j.msea.2014.10.006.
14. D. Xinjie, Z. Zhonga, C. Denga, D. Wanga, X. Guoc: Materials Design, 95, 2016, 231-236. https://doi.org/10.1016/j.matdes.2016.01.087.
15. P. Gawde, R. Kishore, A. Pappachan, G. Kale, G. K. Dey: Transactions of the Indian Institute of Metals, 63, 2010, 853-857. https://doi.org/10.1007/s12666-010-0130-x.
16. V. Tsakiris, M. Lucaci, L. Leonat, G. Alecu: Revista Română de Materiale / Romanian Journal of Materials, 38 (2), 2008, 281–290. https://www.academia.edu/1232165.
17. G. Çam, U. Özdemir,V. Ventzke, M. Koçak: Journal of Materials Science, 43, 2008, 3491-3499. https://doi.org/10.1007/s10853-007-2403-2.
18. N.F. Kazakov: *Diffusion Bonding of Materials*, Mir Publishers, Moscow, 1985.
19. Anon: *Welding Fundamentals and Processes*. Materials Park, Ohio,ASM International, 2011, 682–689.
20. D. J. Stephenson, J. David: *Diffusion Bonding 2*, Elsevier Apllied Science, London and New York, 1991.
21. G. Sharma, L. Tiwari, D. K. Dwivedi: Transactions of the Indian Institute of Metals, 71(1), 2018, 11–21. https://doi.org/10.1007/s12666-017-1136-4.
22. R. Dixon, D. LeRoy Olson, A.Thomas, L. Stephen, R. Edwards: *ASMHandbook Welding*, 6, 1993, 141–142. https://doi.org/10.31399/asm.hb.v06.a0001347.
23. B. Derby, E. R. Wallach: Journal of Materials Science 19, 1984, 3149-3158. https://doi.org/10.1007/BF00549798.
24. N. Masahashi, K. Komatsu, S. Watanabe, S. Hanada: Journal of Materials Science, 41, 2006, 1691–1696. http://dx.doi.org/10.1007/s10853-006-2934-y.
25. S. Li, Q. D. Zhang, J. Y. Liu**:** Strength of Materials, 50, 2018, 818–823. http://dx.doi.org/10.1007/s11223-018-0027-1.
26. M.J. Cox, M.J. Kim, and R.W. Carpenter: Metallurgical and Materials Transactions A, 33, 2002, 437-442. https://doi.org/10.1007/s11661-002-0104-7.
27. B. Kurta, A. Çalik: Materials Characterization, 60, 2009, 1035-1040. https://doi.org/10.1016/j.matchar.2009.04.011.
28. L. Shiwei, S. Xianjun, D.Yajie, Y. Peng, Y. Chen, L. Zhaoxi, J. Xiong, L. Jinglong: Crystals, 11, 2021, 1127. https://doi.org/10.3390/cryst11091127.
29. V. Raghavan: *Materials Science and Engineering: A First Course,*Fifth Edition, PHI learning, New Delhi, 2004.
30. J.C. Zhao: Materials Science Studies, 2005, 1-13. https://doi.org/10.1016/B0-08-043152-6/02041-6.
31. B. Belkessa, D. Miroud, B. Cheniti, N. Ouali, M. Hakem, M. Djama: Diffusion Foundations, 18, 2018, 7-13. https://doi.org/10.4028/www.scientific.net/DF.18.7.

32. K. Arioka, Y. Iijima, T. Miyamoto**:** Philosophical Magazine, 95(32), 2015, 1-13**.**
http://dx.doi.org/10.1080/14786435.2015.1091108.
33. T. Vigraman, R. Narayanasamy, D. Ravindran: Materials and Design, 35, 2012, 156-169.
https://doi.org/10.1016/j.matdes.2011.09.063.
34. H. Yu, C. Jianguo, Y. Liming, S. Yonghong, L. Chenxi, L. Huijun, L. Yongchang: Acta Metallurgica Sinica, 58(2), 2022, 141-154. https://doi.org/10.11900/0412.1961.2020.00446.
35. R.G. Thiessen, I.M. Richardson, J. Sietsma: Materials Science and Engineering A, 427, 2006, 223-231.
https://doi.org/10.1016/j.msea.2006.04.076.